Sequential peripheral enrichment of H2A.Zac and H3K9me2 during trophoblast differentiation in human embryonic stem cells

AUTHOR(S):

Kafer, Georgia Rose; Tanaka, Yoshihisa; Rillo-Bohn, Regina; Shimizu, Eiko; Hasegawa, Kouichi; Carlton, Peter M.

CITATION:

Kafer, Georgia Rose ...[et al]. Sequential peripheral enrichment of H2A.Zac and H3K9me2 during trophoblast differentiation in human embryonic stem cells. Journal of Cell Science 2020, 133(24): jcs245282.

ISSUE DATE:

2020-11-16

URL:

http://hdl.handle.net/2433/260843

© 2020. Published by The Company of Biologists Ltd | Journal of Cell Science (2020) 133, jcs245282. doi:10.1242/jcs.245282

RESEARCH ARTICLE

Sequential peripheral enrichment of H2A.Zac and H3K9me2 during trophoblast differentiation in human embryonic stem cells

Georgia Rose Kafer*, Yoshihisa Tanaka‡, Regina Rillo-Bohn§, Eiko Shimizu, Kouichi Hasegawa and Peter M. Carlton¶,**

ABSTRACT

During the transition from pluripotency to a lineage-committed state, chromatin undergoes large-scale changes in structure, involving covalent modification of histone tails, use of histone variants and gene position changes with respect to the nuclear periphery. Here, using high-resolution microscopy and quantitative image analysis, we surveyed a panel of histone modifications for changes in nuclear peripheral enrichment during differentiation of human embryonic stem cells to a trophoblast-like lineage. We found two dynamic modifications at the nuclear periphery, acetylation of histone H2A.Z (H2A.Zac), and dimethylation of histone H3 at lysine 9 (H3K9me2). We demonstrate successive peripheral enrichment of these markers, with H2A.Zac followed by H3K9me2, over the course of 4 days. We find that H3K9me2 increases concomitantly with, but independently of, expression of lamin A, since deletion of lamin A did not affect H3K9me2 enrichment. We further show that inhibition of histone deacetylases causes persistent and increased H2A.Z acetylation at the periphery, delayed H3K9me2 enrichment and failure to differentiate. Our results show a concerted change in the nature of peripheral chromatin occurs upon differentiation into the trophoblast state.

KEY WORDS: Chromatin, Differentiation, Human embryonic stem cells, Quantitative microscopy, Trophoblast

INTRODUCTION

Pluripotent cell differentiation is accompanied by extensive changes in the expression of pluripotency and lineage-specific genes. Gene expression changes are controlled in turn by several mechanisms, including differential activity of transcription factors, covalent modifications of DNA or chromatin, and movement of gene loci into silent or active nuclear compartments (Peric-Hupkes et al., 2010). While our understanding of the transcriptional networks required for the stem cell state and commitment to a variety of lineages is well developed (Niwa, 2014), our knowledge regarding the role of chromatin changes and nuclear subcompartments in differentiation is not as comprehensive. Some clues have emerged from work on mouse embryonic stem cells (mESCs), where upon differentiation, genes that are required in the newly established cell lineages shift from being late replicating to earlier replicating (Hiratani et al., 2008; Therizols et al., 2014). This shift in replication timing also correlates with dissociation from the nuclear periphery during differentiation, since DNA at the periphery tends to be replicated later than active euchromatic regions (O'Keefe et al., 1992; Peric-Hupkes et al., 2010). The nuclear periphery is in general a gene-repressive compartment (Akhtar and Gasser, 2007); however, no universal causal relationship between gene position and transcriptional state has been defined. Movement of genes to and from the nuclear periphery is influenced by the covalent modification of histone proteins (Kind et al., 2013); association of heterochromatin with the nuclear periphery is especially strongly correlated with dimethylation of histone H3 at lysine 9 (H3K9me2) (Harr et al., 2015; Padeken and Heun, 2014; Puckelwartz et al., 2011; Towbin et al., 2012). H3K9me2-marked chromatin can undergo dynamic relocalization to and from the nuclear periphery in a lineage-specific manner during differentiation (See et al., 2019). The nuclear lamina, a meshwork at the nuclear periphery, is composed of lamin A, its splice variant lamin C (collectively lamin A/C), lamin B and their interacting proteins. Of these, lamin A/C and the lamin B receptor (LBR), have been strongly implicated in anchoring heterochromatin to the nuclear periphery in multiple cell types (Solovei et al., 2013). While lamin A and C make up the bulk of the nuclear lamina in differentiated cells, these are only expressed at low levels in pluripotent cells; consequently, the lamina in pluripotent cells is composed largely of only lamin B. Whether the low level of lamin A present in undifferentiated human ESCs plays a role in transcriptional control is not clear.

Several reports have shown that the differentiation of stem cells is accompanied by significant changes in covalent DNA and histone protein modification, which influence the activity of genes (Kim et al., 2011; Sachs et al., 2013). H3K9 di- or tri-methylation is consistently associated with transcriptional repression, and targets lineage-associated genes during differentiation (Chen et al., 2012). Large H3K9me2 domains are present in both undifferentiated and differentiated cells (Lienert et al., 2011), but these undergo dynamic changes at the local level during differentiation. H2A.Z is a histone variant whose many roles are modulated by post-translational modifications, and is exchanged for canonical H2A by the Tip60 complex. While H2A.Z itself has been found in both repressive and activating contexts (Giaimo et al., 2019), its acetylated form has exclusively been found to be correlated with gene activation (Bruce et al., 2005; Keogh et al., 2006; Valdés-Mora et al., 2017). Global and predictable changes in chromatin modifications between different nuclear compartments in differentiated and undifferentiated stem cells have also been reported (Bártová et al., 2008). Despite these studies, we still know little about the kinetics of establishing chromatin environments during lineage commitment. Especially, the

Institute for Integrated Cell-Material Sciences (iCeMS), Kyoto University, Kyoto 606-8501, Japan.
*Present address: Genome Integrity Unit, The Children's Medical Research Institute, Westmead, NSW 2145, Australia. ‡Present address: Graduate School of Pharmaceutical Sciences, Kyoto University, Kyoto 606-8501, Japan. §Present address: Department of Microbiology and Molecular Genetics, University of California Davis, Davis 95616, USA. ¶Present address: Graduate School of Biostudies, Kyoto University; and Radiation Biology Center, Kyoto University, Kyoto 606-8501, Japan.

**Author for correspondence (carlton.petermark.3v@kyoto-u.ac.jp)

G.R.K., 0000-0002-5438-0497; P.M.C., 0000-0002-5320-6024

Handling Editor: Caroline Hill
Received 16 February 2020; Accepted 27 October 2020

Journal of Cell Science (2020) 133, jcs245282. doi:10.1242/jcs.245282

relationship between chromatin modifications and different nuclear compartments in cells at intermediate states between pluripotency and terminal differentiation is not understood well. Further, ensembles of cells can yield information about chromatin changes at high genomic resolution, but not 3D nuclear architecture of individual cells.

Trophoblast cells are the first cells to terminally differentiate *in vivo*, and eventually make up the extraembryonic placental tissue. Trophoblast-like (TBL) cells can be effectively and homogeneously differentiated from human embryonic stem cells (hESCs) through treatment with BMP4 and simultaneous inhibition of FGF and activin/nodal signaling (Amita et al., 2013; Sudheer et al., 2012). Compared to other commonly employed differentiation pathways to generate neural progenitor or mesoderm lineages, TBL differentiation generates cells that are immediately terminally committed, finish differentiation in less than 1 week, and exhibit characteristic chromatin states, including significant hypomethylation and distinct chromatin organization in a highly homogeneous manner (Kar et al., 2007; Mori et al., 2007; Schroeder et al., 2013). The fast, unidirectional and homogeneous nature of TBL cell differentiation provides a tool to study cellular events that happen immediately upon loss of pluripotency.

In this study, we have analyzed individual hESCs to assay the localization of modified histones with respect to the nuclear periphery during the early phases of pluripotency loss and into the beginning stages of terminal lineage commitment to TBL cells. We visualized histone modifications with immunofluorescence using high-resolution microscopy, and quantitatively analyzed the three-dimensional (3D) nuclear distribution of histone modifications relative to the nuclear periphery. To this end, we developed an automated program that recognizes and crops individual nuclei in three dimensions, and executes a shell analysis to quantitatively examine distance-dependent distribution patterns of histone modifications relative to the nuclear periphery in hundreds of cells. Our shell analysis program is applicable to many different types of cells and signals whose distribution relative to nuclear periphery are to be determined. We surveyed dynamic changes of modified chromatin (H3K4me3, H3K9me2, H3K9me3, H3K27ac, H3K27me3 and H3K36me3) and one histone variant (H2A.Z) and its acetylated form (H2A.Zac) in hESCs from both primed and ‘naïve’ pluripotent states (Gafni et al., 2013; Warrier et al., 2017) in addition to hESCs which are differentiating to the trophoblast lineage. We show that two histone modifications, H3K9me2 and H2A.Zac, show changes in their distribution at the nuclear periphery as hESCs transition from naïve to primed and a differentiated trophoblast state. Particularly, we have captured transient association of H2A.Zac with the nuclear periphery within 12 h upon loss of pluripotency, and found that this coincides with the transient loss of H3K9me2 from the nuclear periphery during the process of hESC differentiation into trophoblast lineages. Our analysis uncovered that transient and dynamic nuclear periphery association of specific histone modifications may occur during intermediate stages of trophoblast differentiation. Such transient changes could be missed by only analyzing cells after the completion of differentiation. Furthermore, we show that HDAC activity is a key controlling factor in the establishment of chromatin environments at the nuclear periphery during differentiation.

RESULTS

Characterization of fast, homogeneous differentiation from hESCs to the TBL lineage

We first characterized the extent to which our TBL induction scheme could produce homogeneous, rapid pluripotency loss and differentiation from hESCs to TBL cells. We subjected primed hESCs to a treatment inducing TBL differentiation, as previously described (Amita et al., 2013; Sudheer et al., 2012) (Fig. 1A, see Materials and Methods) and observed changes in gross cellular morphology, as well as the development of characteristic chromatin morphology revealed by DAPI staining (Fig. 1B). This DAPI morphology is qualitatively similar to that seen in early human placental sections (Mori et al., 2007). Pluripotency loss was confirmed by a rapid drop in OCT3/4 (also known as POU5F1) levels upon differentiation induction (Fig. 1C). Immunofluorescence indicated that TBL induction caused a drop in NANOG and OCT3/4 (POU5F1) levels within 24 h (Fig. 1D), and single-molecule fluorescence *in situ* hybridization (FISH) confirmed that *NANOG* mRNA levels were downregulated at this time (Fig. 1E). The mRNA for *CDX2*, a gene essential for placental development (Chawengsaksophak et al., 2004), was detectable 48 h post induction and was specifically detected in a subset of cells at 96 h that displayed DNA morphology qualitatively similar to *in vivo* human cytotrophoblasts (Mori et al., 2007) (Fig. 1F). Immunofluorescence also demonstrated that the trophoblast-specific marker cytokeratin 7 was expressed in cells possessing the cytotrophoblast-like DNA morphology at 4 and 6 days post induction (Fig. S1A), as were other human trophoblast markers such as GCM1, SYNA and human chorionic gonadotropin (hCG) (Fig. S1B). Lamin A, a nuclear envelope protein that is not abundantly expressed in pluripotent hESCs (Constantinescu et al., 2006) and shows extremely sparse staining in undifferentiated hESCs, became clearly detectable at the nuclear periphery 48 h after TBL induction (Fig. 1G). Taken together, these results indicate our differentiation scheme is capable of rapid and homogeneous trophoblast differentiation as measured through these cell fate markers.

H2A.Zac and H3K9me2 undergo waves of relocation at the nuclear periphery as hESCs lose pluripotency and differentiate into trophoblast cells

We reasoned that if both subnuclear position and covalent histone modifications were involved in modulating gene expression, then subnuclear changes in histone modification should be cytologically visible across a differentiation time course. Using immunofluorescence, we examined the intensity and localization pattern of several histone modification marks associated with either active (H3K4me3 and H3K27ac) or inactive chromatin (H3K9me2, H3K9me3, H3K27me3 and H3K36me3) (Bártová et al., 2008) as well as one histone variant (H2A.Z) and its acetylated form (H2A.Zac), which have been associated both with activation and repression in different contexts (Giamo et al., 2019), in primed hESCs and at 24 h post-TBL induction (Fig. 2). The subnuclear distribution of pan-H2A.Z, H3K4me3, H3K36me3, H3K27ac, H3K27me3 and H3K9me3 did not noticeably change following 24 h of differentiation (Fig. 2A,C–F,H).

In contrast, two of the tested histone modifications, H2A.Zac and H3K9me2, showed marked changes in nuclear distribution as cells lost pluripotency. Under hESC conditions, H2A.Zac was distributed evenly throughout the nucleus. After 24 h of differentiation, the H2A.Zac signal appeared enriched at the nuclear periphery but was reduced in the nucleoplasm (Fig. 2B). Interestingly, H3K9me2 signals appeared to change in a manner opposite to that of H2A.Zac; undifferentiated hESCs displayed enriched H3K9me2 at the nuclear periphery, which was lost 24 h after differentiation (Fig. 2G).

To fully characterize H2A.Zac and H3K9me2 dynamics across all hESC stages, we took samples at 12, 24, 48 and 96 h after the commencement of differentiation. We carried out peptide competition immunofluorescence (Poleshko et al., 2019) to ensure the specificity of our antibodies in immunofluorescence (Fig. S2);

Journal of Cell Science (2020) 133, jcs245282. doi:10.1242/jcs.245282

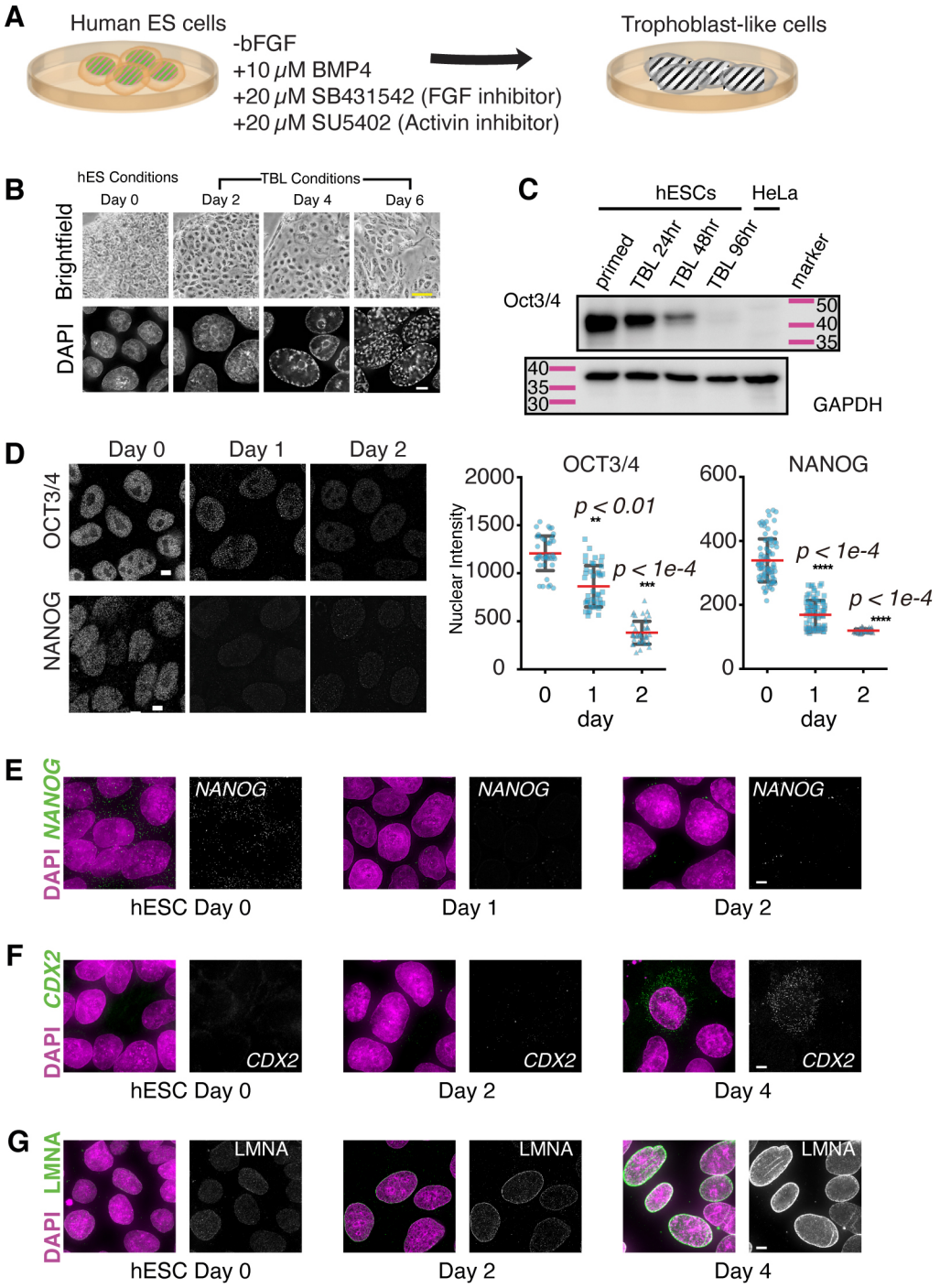

Fig. 1. Changes in morphology and gene expression of human embryonic stem cells during differentiation to a trophoblast-like state. (A) Schematic of the differentiation procedure. (B) Changes in colony morphology, nuclear staining using DAPI, and pluripotency markers OCT3/4 and NANOG as determined using immunofluorescence, during differentiation. Scale bars: 50 µm (top), 5 µm (bottom). (C) Western blots showing OCT3/4 protein amounts at 0, 1, 2 and 4 days post differentiation and in HeLa cells. The lower GAPDH loading control is a separate blot using equal amounts of the same lysate as the above blot. (D) Images and quantification of intensity levels of OCT3/4 and NANOG; red lines show mean intensity values and bars extend to one standard deviation; *P*-values for difference of mean value compared to day 0 are shown (*t*-test). (E,F) Single-molecule FISH against (E) *NANOG* mRNA and (F) *CDX2* mRNA is shown in green. DAPI staining is in magenta. (G) Immunofluorescence against lamin A (LMNA) is shown in green. DAPI staining us in magenta. Scale bars: 5 µm.

others have independently shown specificity for the same antibodies (Valdés-Mora et al., 2017). To determine whether the pattern of histone modifications in non-differentiated hESC is characteristic of the primed state and the naïve state (a distinct, developmentally earlier, state of pluripotency in which cells are less prone to differentiate), we compared conventionally cultured primed hESCs to naïve hESCs. To quantitatively assess the apparent enrichment of signals at the nuclear periphery by immunofluorescence, we implemented a shell averaging program operating on 3D images (Fig. 3A). The source images for the program are 3D fields of ∼15 µm depth containing 2–10 cell nuclei. The DAPI channel is used to automatically segment each nucleus into its own new image, and is also used to define the nuclear periphery. The mid-section of each nucleus is automatically detected, and fluorescence intensity is then averaged in all channels inside each of a series of twenty concentric shells reaching from 0.5 µm outside the nuclear periphery to ∼1.5 µm inside, in five *Z*-sections surrounding the midsection. The shells intentionally begin outside the true nuclear periphery, to create a detectable peak in the nuclear signal. For each experiment, a montage of all segmented nuclei is automatically generated, which is used to visually exclude instances of failed segmentation (e.g. partial nuclei, or several nearby nuclei being falsely detected as a single nucleus).

For each experiment, cells were fixed at various time points and kept at 4°C; immunostaining of all samples was then conducted at

Journal of Cell Science (2020) 133, jcs245282. doi:10.1242/jcs.245282

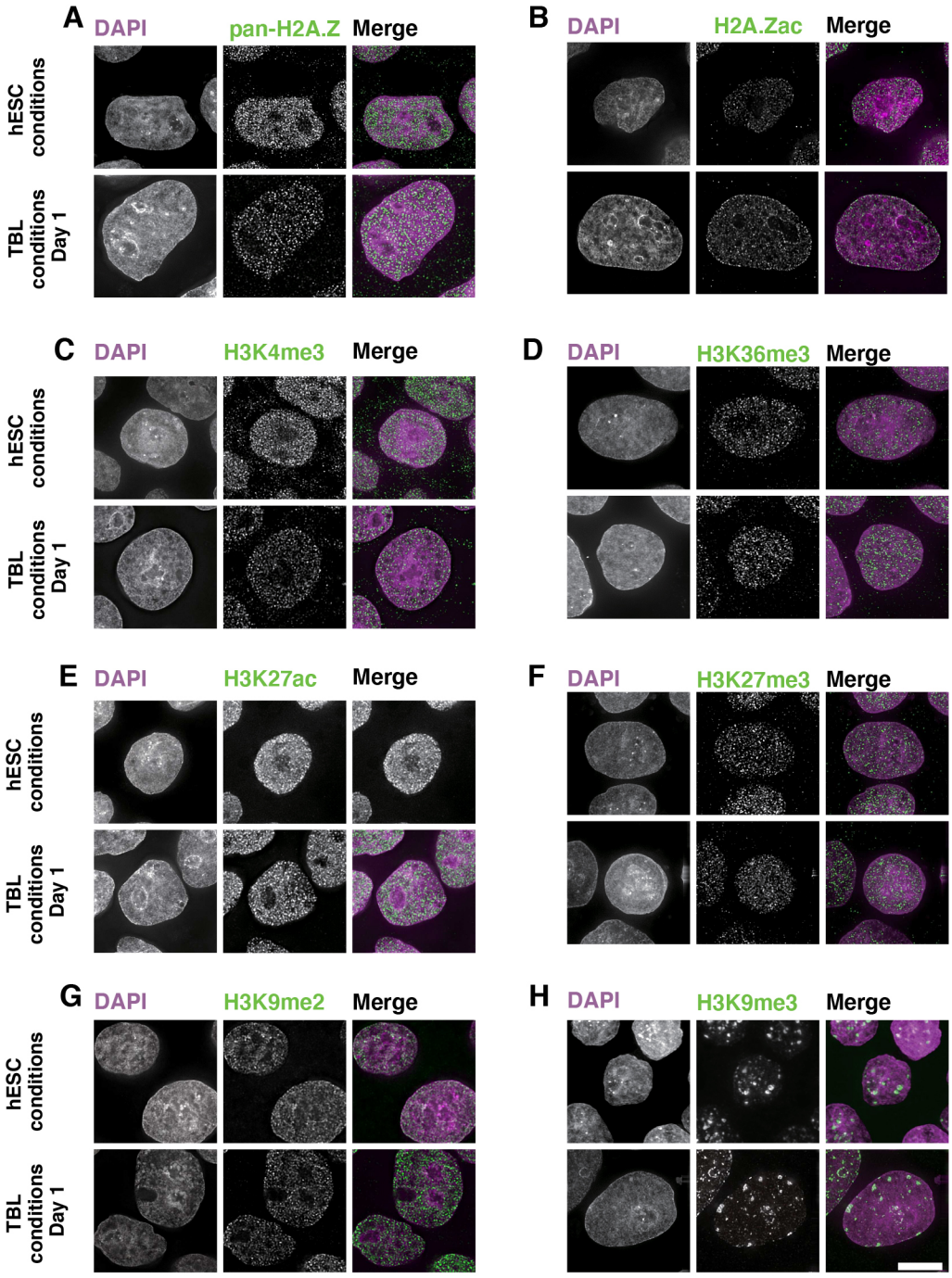

Fig. 2. Chromatin markers display dynamic changes during differentiation. All panel sets show single *Z*-sections of primed hESCs (top) or hESCs 24 h after changing to TBL differentiation medium (bottom). Cells were stained with antibodies against the indicated chromatin markers. DAPI staining is shown in grayscale and magenta in the merged column; the various chromatin markers are shown in grayscale and green in the merged column. Scale bar: 5 µm.

the same time (day 4) to minimize technical variability. Images were acquired with the same exposure time in each wavelength to facilitate direct comparisons, and at least 90 cells total were analyzed from two or three biological replicates in all cases. The reliability of this method was confirmed by a consistent 200 nm average peak distance measured between the peak of lamin A/C immunostaining and the peak of DAPI staining in differentiated cells, identical to that obtained using manual inspection (Fig. S3). Using this method, we found that H2A.Zac was initially diffuse in naïve hESCs, but in primed hESCs, H2A.Zac was found more strongly throughout the nucleus and was occasionally enriched at the nuclear periphery (Fig. 3B). At 12 h post-TBL induction, most hESCs showed strong peripheral enrichment of H2A.Zac, while internal levels declined. After 24 h of trophoblast differentiation, cells still exhibited H2A.Zac enrichment at the nuclear periphery, but peripheral levels appeared reduced compared to cells at 12 h. At 48 h post differentiation, most nuclei no longer displayed peripherally enriched H2A.Zac, and by 96 h, the H2A.Zac signal became very low throughout the whole nucleus. Peripheral shell analysis across the population demonstrated that there were some cells with peripheral H2A.Zac enrichment at all time points assayed, but at 12 and 24 h post differentiation the majority of the population exhibited peripheral H2A.Zac (Fig. 3B,C).

To test whether peripheral enrichment was specific to the acetylated version of H2A.Z, we also characterized pan-H2A.Z dynamics. In both naïve and primed hESC pan-H2A.Z was seen as

Journal of Cell Science (2020) 133, jcs245282. doi:10.1242/jcs.245282

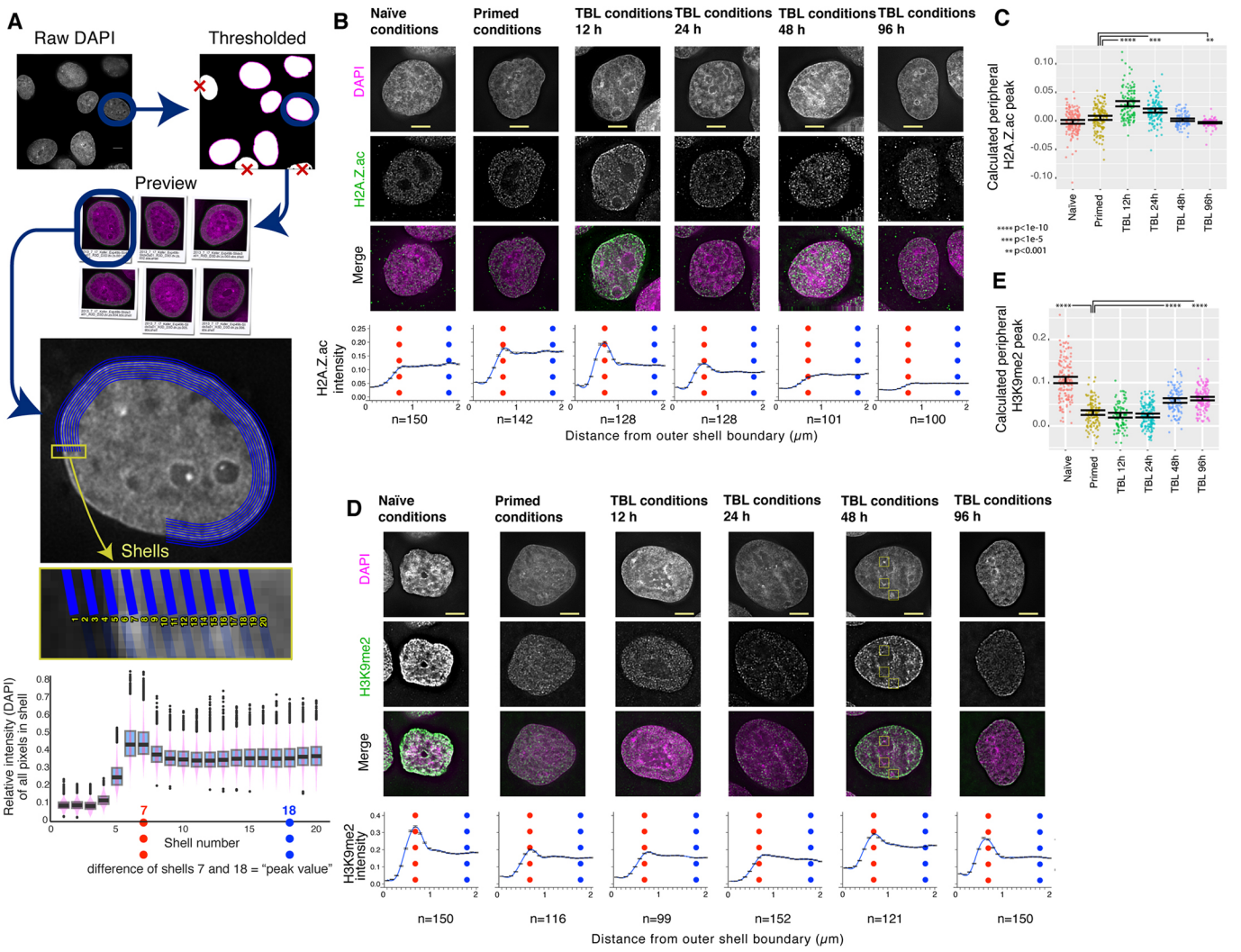

Fig. 3. H2A.Z acetylation and H3K9me2 are alternately enriched at the nuclear periphery during differentiation. (A) Illustration of the shell-averaging procedure. The DAPI image is used to define a set of concentric shells spanning the nuclear periphery. The intensity of chromatin markers (or DAPI, shown here for illustration) within each shell is averaged for the number of cells indicated underneath each graph; the difference between shells 7 and 18 is used to calculate the peak value. Graph shows a box plot where the box represents the 25–75th percentiles, and the median is indicated. The entire range of data is shown by violin plots (magenta) and outliers are shown by gray circles. (B) Immunofluorescence examples of H2A.Zac under different differentiation conditions (top) and plots of shell-averaged intensity. Cells shown are from representative fields. Line graphs shown are those from cells nearest the average peak value for their class. Error bars indicate the s.e.m. of intensity values at each shell position; red and blue dotted lines indicate the peak shell position (shell#7) and an internal shell position (#18) used for normalization. (C) Plots of peripheral peak values of H2A.Zac for all cells. *n*=150, 150, 128, 128, 101, 100 from left to right. (D) Immunofluorescence examples of H3K9me2 and corresponding plots, under the same conditions shown in B. Yellow boxes surround regions of increased DAPI intensity that do not show corresponding increases of H3K9me2 immunofluorescence signal. (E) Plots of peripheral peak values of H3K9me2 for all cells *n*=150, 116, 99, 152, 121, 150 cells from left to right. For C and E, error bars show 95% confidence interval of the mean value. $^{**}P<0.001$; $^{***}P<10^{-5}$; $^{****}P<10^{-10}$ (difference of means test between each condition and the 'primed' hESC condition after correction for multiple comparisons). Scale bars: 5 µm.

small nucleoplasmic foci that were present throughout the nucleus, although these were qualitatively more intense in primed cells (Fig. S4). After 24 h of TBL induction, pan-H2A.Z levels remained high in the nucleoplasm, but further differentiation was accompanied by a decrease back to naïve levels. While pan-H2A.Z detected by immunofluorescence also changed dynamically, it was not enriched at the nuclear periphery, indicating that the periphery is specifically enriched for acetylation of H2A.Z.

We next assayed H3K9me2 dynamics across the 4-day trophoblast differentiation time course. We found that H3K9me2 appeared at the nuclear periphery in a pattern strikingly opposite to that seen for H2A.Zac. H3K9me2 was significantly peripheral in naïve cells, reaching peak intensity within 0.7 µm from the thresholded nuclear periphery (Fig. 3D), the same shell as the peak of DAPI intensity due to peripheral heterochromatin. The fact that DAPI staining also shows a prominent peak at the periphery means that DNA itself is likely somewhat enriched at the nuclear periphery, meaning that enrichment assayed by this method should be understood as being relative to that seen at other time points or with other histone modifications that do not show such enrichment. However, DAPI and histone marks show divergence in their intensity patterns (boxes in Fig. 3D), indicating that DNA density does not solely determine enrichment of modified histones. Peripheral enrichment was reduced in primed hESCs relative to in naïve hESCs nuclei, and by 12 h following the initiation of differentiation, the peripheral H3K9me2 signal was significantly

Journal of Cell Science (2020) 133, jcs245282. doi:10.1242/jcs.245282

reduced (Fig. 3D,E). The nucleoplasmic H3K9me2 signal returned at 24 h post differentiation and, from 48 h, cells again exhibited a robust H3K9me2 signal at the nuclear periphery (Fig. 3D). Population-wide peripheral shell analysis revealed that primed hESC and cells at 12 and 24 h of differentiation displayed reduced H3K9me2 signal at the nuclear periphery relative to populations of both naïve cells and cells that had been undergoing trophoblast differentiation for 48 h or more (Fig. 3E).

We next investigated whether any correlation existed between the levels of H2A.Zac and H3K9me2 at the nuclear periphery, and how these changes related to pluripotency loss. We performed simultaneous immunostaining of H2A.Zac and H3K9me2 with lamin A/C. We located cells that still possessed some peripheral enrichment for H2A.Zac at 24 h post differentiation, and compared their peripheral profiles to neighboring cells in the same image that had undergone H2A.Zac reduction. In these cells, we qualitatively found a positive relation between H2A.Zac reduction, H3K9me2 accumulation, and differentiation status as judged by the intensity of the peripheral lamin A border (Fig. 4).

Lamin A is not necessary for peripheral chromatin reorganization during hESC differentiation into trophoblasts

Given that the gradual expression and localization of lamin A at 48 h after TBL differentiation coincides with re-appearance of H3K9me2 at the periphery, we hypothesized that lamin A might be a factor influencing the dynamic changes of H3K9me2 localization to the nuclear periphery. To test this, we used CRISPR to generate a hESC line with a homozygously disrupted *Lmna* gene in which neither lamin A nor C are expressed (Fig. 5A). *Lmna*$^{-/-}$ hES cells proliferated normally, as judged by similar times to reach confluency after passaging, and appeared roughly the same as control cells under normal culturing conditions (Fig. S5). Immunofluorescence microscopy showed a complete loss of lamin A/C staining in knockout cells, in contrast to the faint but distinct nuclear rim staining visible in unedited cells (Fig. 5B). Despite the loss of lamin A, no differences in H3K9me2 localization or peripheral enrichment could be seen between homozygous knockout and unedited cells (Fig. 5C,D). *Lmna*$^{-/-}$ hESCs were also able to differentiate into other lineages, including beating cardiomyocytes and neuro-progenitor cells (NPCs) by directed differentiation induction (Movie 1 and data not shown). We therefore conclude that although lamin A localization in hESCs is highly correlated with H3K9me2 at the periphery, it is not required for its localization.

The localization of HAT and HDAC proteins is dynamic as hESCs differentiate

We next wondered how H2A.Zac levels were changed by acetylation [i.e. histone acetyltransferase (HAT) activity] versus deacetylation [i.e. histone deacetylase (HDAC) activity]. We reasoned that if histone modifications were enriched at the nuclear periphery, then the enzymes responsible for them may also be cytologically detectable in the same location. Previous work suggests that Tip60 (also known as KAT5) is the primary HAT catalyzing H2A.Z acetylation (Auger et al., 2008; Ito et al., 2018; Keogh et al., 2006), and while the identity of HDACs responsible for deacetylation of H2A.Zac is not known, it is likely to be a member of the 'class I' HDACs, that is, HDAC1, HDAC2 or HDAC3 (Delcuve et al., 2012). HDAC1 and HDAC2 are known to be required for self-renewal and differentiation in ESCs and trophoblast stem cells; however, the role of HDAC1 seems to be more critical (Dovey et al., 2010; Jamaladdin et al., 2014; Kidder and Palmer, 2012).

We found that in primed hESCs, Tip60 existed in three primary patterns, as central nucleoplasmic clusters surrounding DAPI-enriched areas, as diffuse nucleoplasmic foci with no clear enrichment pattern, or as nucleoplasmic foci with a tendency for enrichment at the nuclear periphery (Fig. S6A). Each specific Tip60

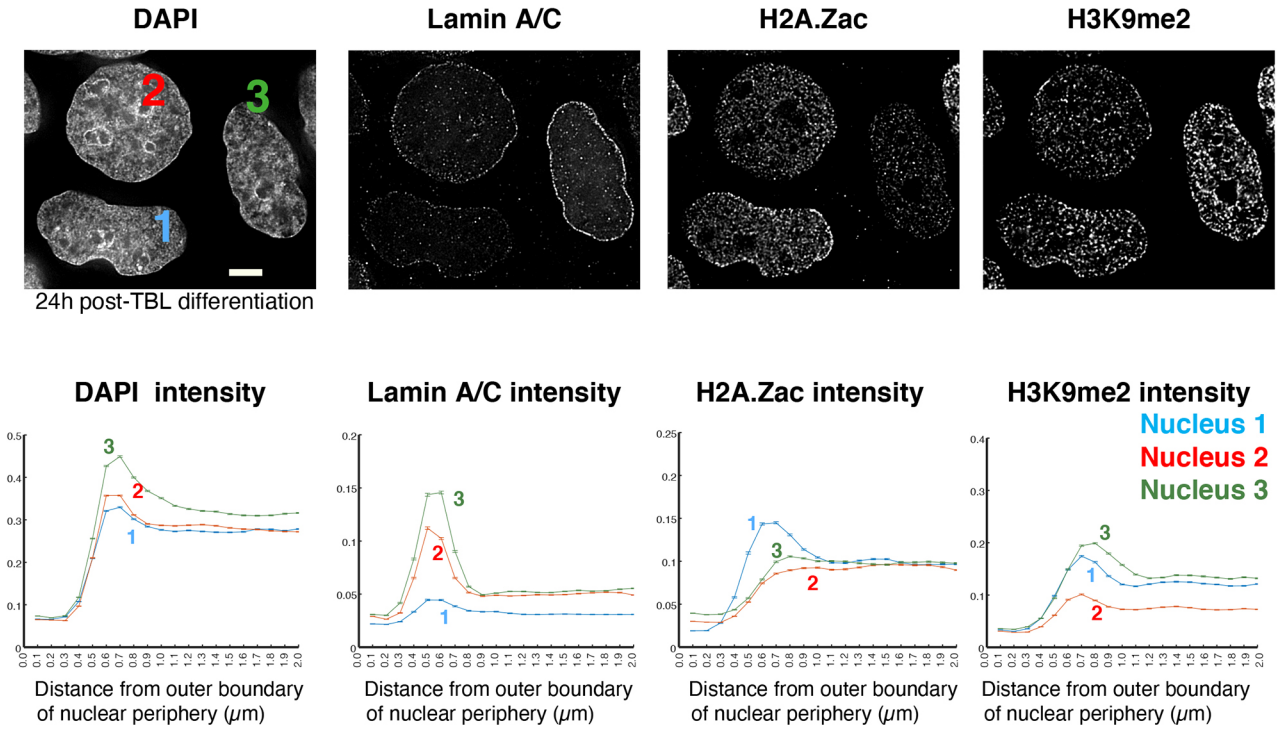

Fig. 4. Comparison of neighboring individual cells at 24 h after commencement of TBL induction shows successive enrichment of H2A.Zac and H3K9me2 peripheral intensity. Cells are shown stained with DAPI and immunofluorescence as indicated; shell-averaged intensity graphs are shown for each numbered cell. Error bars indicate the s.e.m. for all pixel intensities in each shell. Scale bar: 5 µm.

Journal of Cell Science (2020) 133, jcs245282. doi:10.1242/jcs.245282

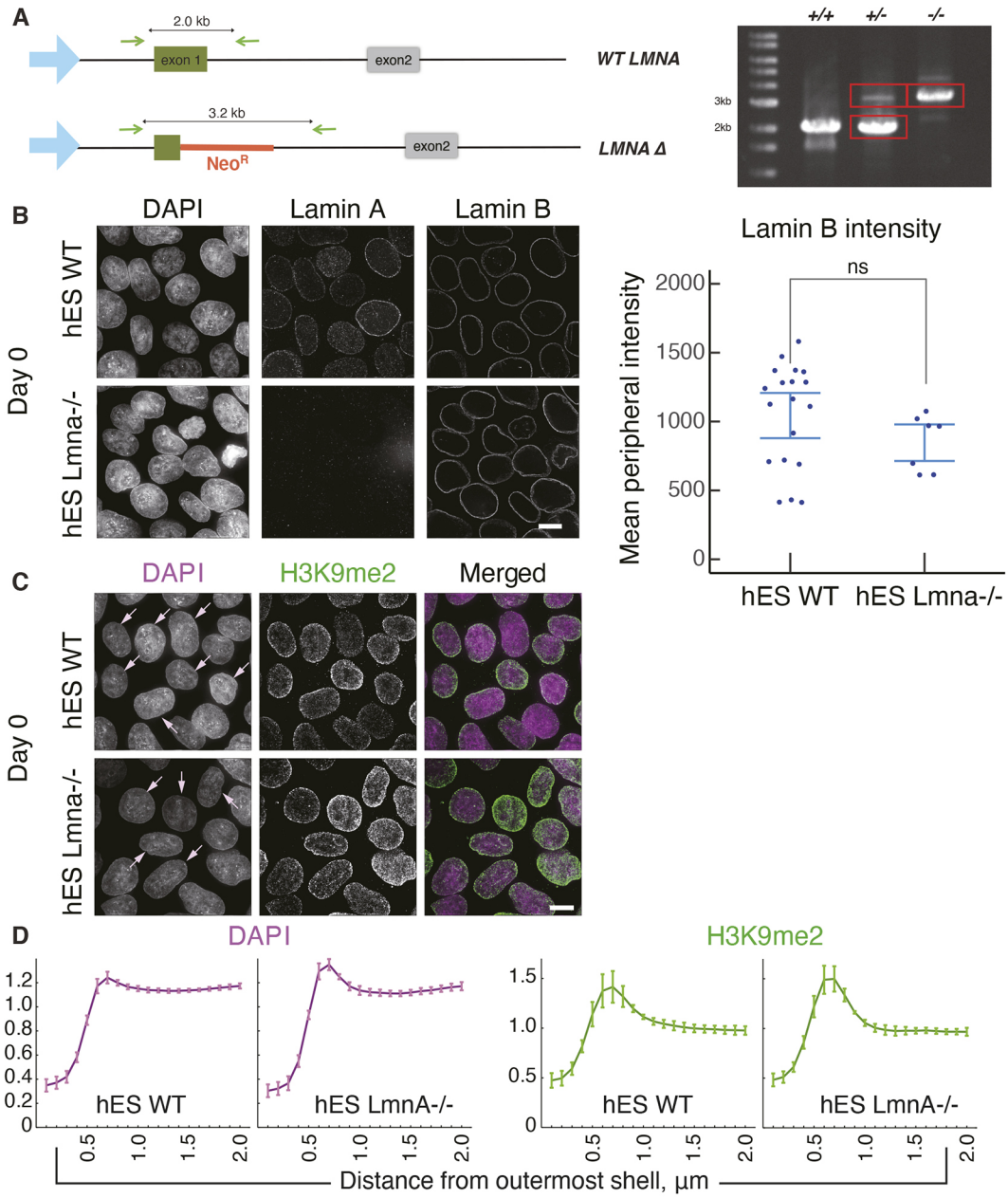

Fig. 5. Lamin A does not play a role in H3K9me2 dynamics during TBL differentiation. (A) Illustration of gene editing to remove the *LMNA* gene. CRISPR was used to replace the first exon of *LMNA* with a neomycin resistance cassette, leading to disruption of the gene; heterozygous and homozygous deletions were detected by PCR as shown (right). (B) WT hESCs (top) and *LMNA*$^{-/-}$ hESCs (bottom) stained for DAPI, lamin A and lamin B. Quantification of the mean peripheral intensity of the lamin B staining (the difference between shell#7 and shell#18) is shown at right, with mean and 95% confidence intervals indicated. ns, not significant (*t*-test). (C) DAPI and H3K9me2 staining in undifferentiated WT hESCs (top) and *LMNA*$^{-/-}$ hESCs (bottom). Arrows indicate cells analyzed below. (D) Quantification of DAPI and H3K9me2 peripheral shell staining in WT hESCs (n=7) and *LMNA*$^{-/-}$ hESCs (n=6) as indicated. Error bars indicate s.e.m. error of pixel intensity values at each shell position. Scale bars: 10 µm.

pattern could be found in cells at 12 h and 24 h post-TBL induction as well; however, the proportion of nuclei possessing different localizations changed, with primed hESCs showing greater tendency toward peripheral localization than naïve or differentiating cells. In contrast, HDAC proteins displayed mostly homogeneous nuclear localization as determined by immunofluorescence. We found that both HDAC1 and HDAC2 were localized to the nucleus in hESCs. HDAC2 was stained intensely in hESC nuclei (Fig. 6A), while HDAC1 presented as small foci throughout the nucleoplasm (Fig. S6B). HDAC1 levels appeared to drop as hESCs began to differentiate (Fig. S6B) while HDAC2 levels were retained throughout differentiation, with increased signal at 12 and 24 h post-TBL induction (Fig. 6B,E).

The modifier specifically responsible for catalyzing H3K9 dimethylation is the histone methyl-transferase (HMTase) G9a (also known as EHMT2) (Tachibana et al., 2002). In primed hESCs, G9a was detected by immunostaining as small foci throughout the cell nucleus (Fig. 6C). G9a location tracked that of H3K9me2 from 24 h post differentiation, with a modest increase in G9a intensity throughout the nucleoplasm and a measurable increase in G9a signal at the nuclear periphery in hESCs at 24 and 48 h post differentiation (Fig. 6D). As judged by western blots from

Journal of Cell Science (2020) 133, jcs245282. doi:10.1242/jcs.245282

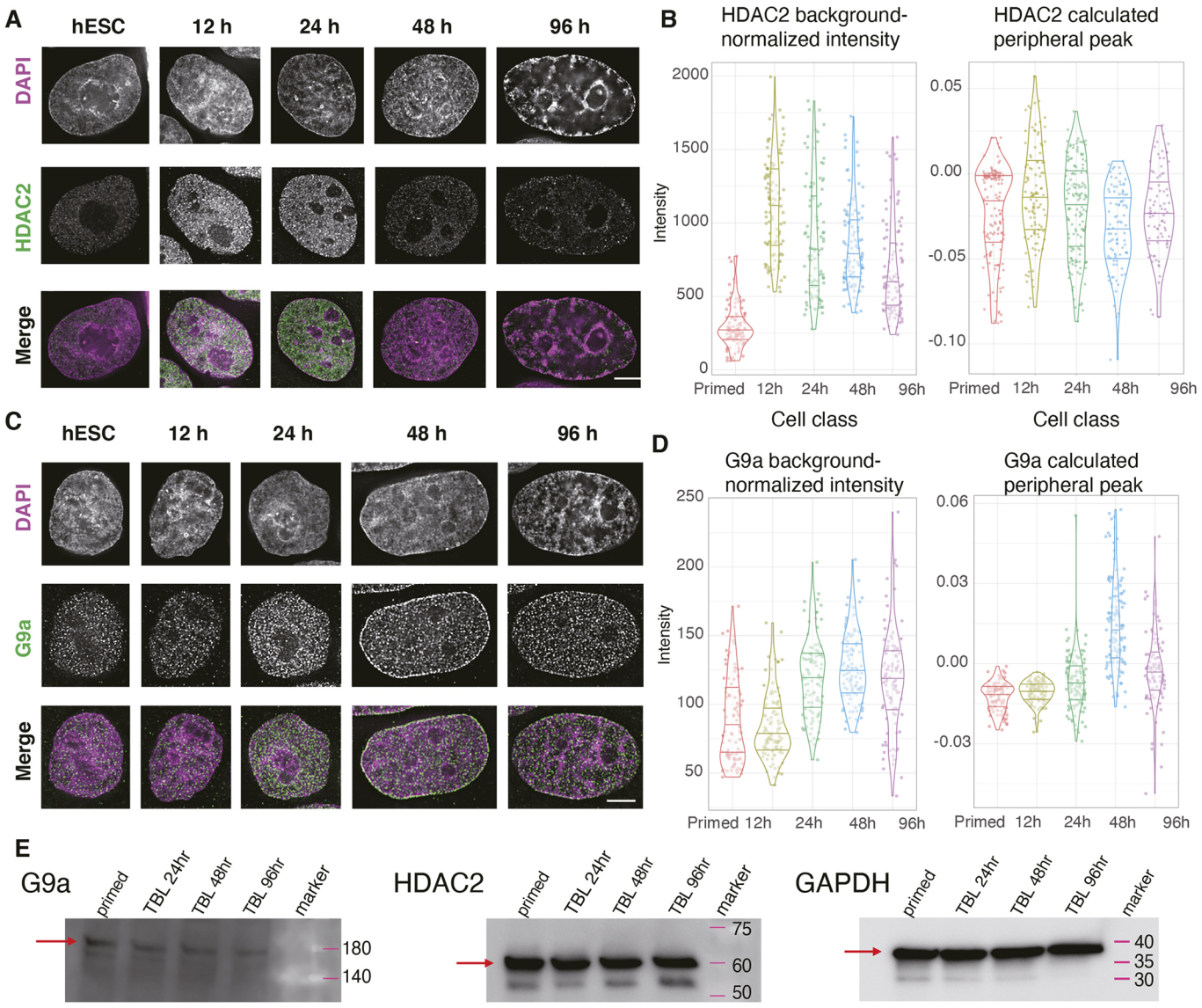

Fig. 6. HDAC2 and G9a display dynamic localization during TBL differentiation. (A) Representative images of HDAC2 immunostaining during a TBL differentiation time course. Images are shown as single sections. Scale bar: 5 µm. (B) Quantifciation of mean background-corrected intensity of HDAC2 for all nuclei at each time point (left) as well as the peak value calculated by subtracting the mean of shell#18 from that of shell#7 (right). All data points are shown as dots; distribution density shown by violin plot with the median and 25 and 75th percentiles indicated. *n*=104, 102, 101, 112, 98 cells measured from left to right. (C) Representative images of G9a immunostaining during TBL differentiation. Images are shown as single sections. Scale bar: 5 µm. (D) Mean background-corrected intensity of G9a as in B for all nuclei at each time point (left) as well as the corresponding peak values (right). For both HDAC2 and G9a, the image chosen for each time point is closest to the mean value for total intensity. *n*=100, 103, 108, 105, 104 cells measured from left to right. (E) Western blots performed on lysates from hESCs at the indicated time points, using antibodies against G9a (left) and HDAC2 (middle). The protein loading control (GAPDH) for these blots was run separately (right) using equal volumes from the same lysates. Protein of interest highlighted by arrow.

whole-cell lysates, however, the overall protein level of G9a, like HDAC2, does not change drastically during the trophoblast differentiation process (Fig. 6E). Together, our data suggests that HAT, HDAC and HMTase complexes responsible for changes in H2A.Z acetylation status and H3K9 methylation status also exhibit some dynamic changes in their localization during pluripotency loss and early phases of trophoblast differentiation.

Peripheral acetylation of H2A.Z and dimethylation of H3K9, as well as trophoblast differentiation, are blocked by TSA treatment

We next asked whether pharmacologically inhibiting histone modification enzymes would affect the localization of histone marks, and subsequently pluripotency loss and/or trophoblast differentiation. We performed a series of experiments using the HDAC inhibitor trichostatin A (TSA), a global inhibitor of class I HDACs (Yoshida et al., 1990), expected to inhibit HDAC1, HDAC2 and HDAC3. Cells were first subjected to TBL differentiation, and then exposed to 12.5 nM TSA for either 12 h or 36 h before sampling; control cells without TSA were sampled in parallel (Fig. 7A). Inhibition with TSA is reversible, and does not alter HDAC protein levels nor association, only deacetylation kinetics (Sekhavat et al., 2007). This allowed us to indirectly interpret gains in histone acetylation in different nuclear compartments as locations where class I HDAC complexes would usually be active (Fig. 7B). To determine whether HDAC activity drives H2A.Zac removal from the nuclear

Journal of Cell Science (2020) 133, jcs245282. doi:10.1242/jcs.245282

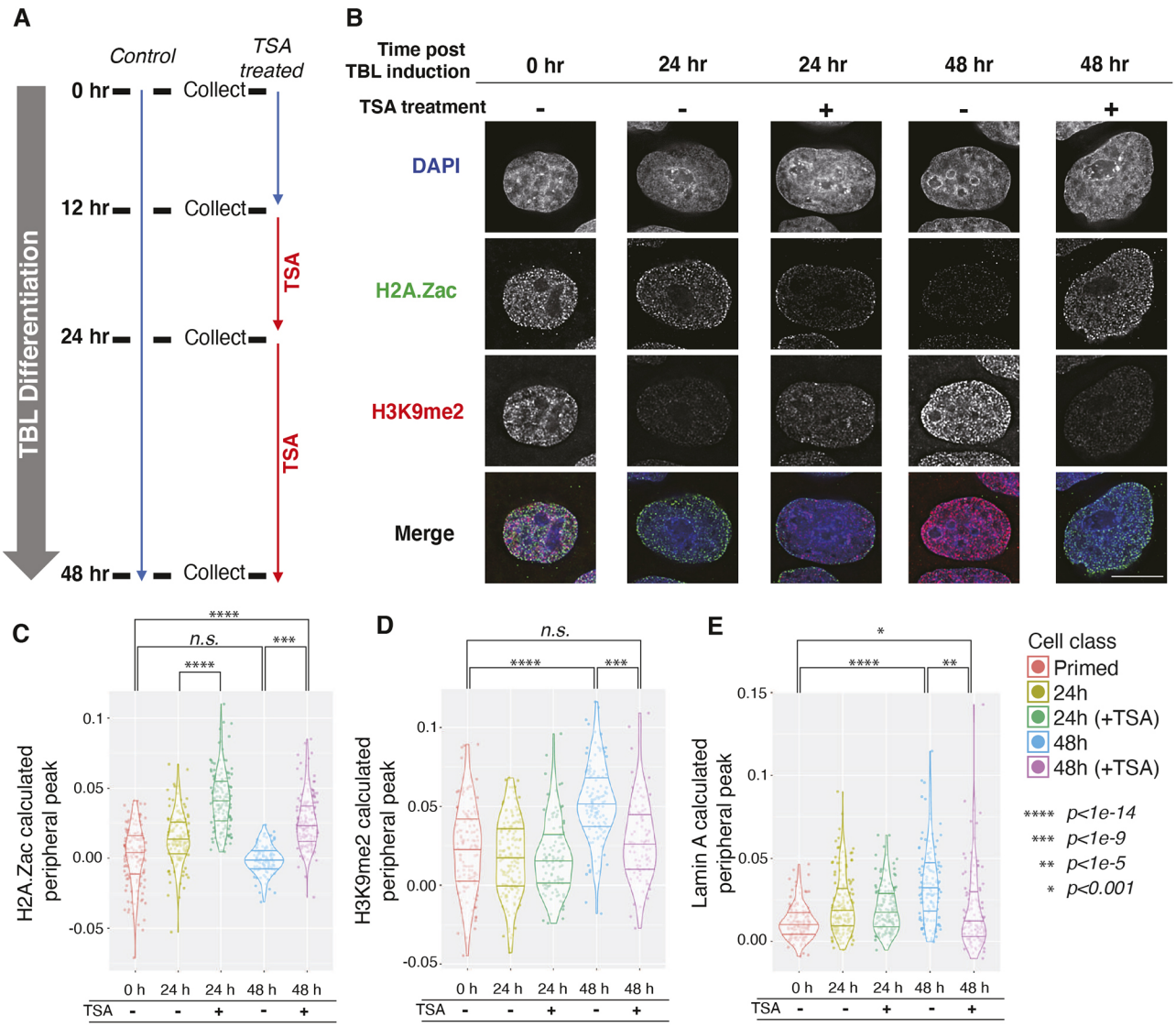

Fig. 7. TSA treatment prevents differentiation-associated changes in H2A.Z acetylation and H3K9 dimethylation. (A) Schematic of treatment and collection times. TBL differentiation begins at time *t*=0. (B) Representative images of nuclei immunostained for H2A.Zac and H3K9me2. (C) Peak values of H2A.Zac calculated for individual cells; *n*=142, 128, 141, 101, 149 from left to right. Scale bar: 5 µm. (D) Peak values of H3K9me2 calculated for individual cells; *n*=116, 153, 102, 121, 81 from left to right. (E) Peak values of lamin A calculated for individual cells; *n*=134, 153, 129, 122, 111 from left to right. Results are shown by violin plot with the median and 25 and 75th percentiles indicated. **P*<0.001; ***P*<10^{-5}; ****P*<10^{-9}; *****P*<10^{-14}; ns, not significant (two-tailed *t*-test).

periphery during trophoblast differentiation, hESCs were induced to differentiate and treated with TSA at 12 h, when peripheral H2A.Zac is elevated yet global levels have begun to decline. Under these conditions, H2A.Zac remained enriched at the nuclear periphery and the H3K9me2 signal at the periphery did not increase even after 48 h of growth under differentiation conditions (Fig. 7C,D). Lamin A at the nuclear periphery was also less intense in treated cells, suggesting that TSA-treated hESC did not differentiate (Fig. 7E). These results suggest that HDAC activity, which appears to drive H2A.Zac removal from the nuclear periphery, is required for the normal progression of trophoblast differentiation.

DISCUSSION

By quantitatively measuring the intranuclear distribution of histone modifications and variants during TBL differentiation, we find that H2A.Zac and H3K9me2 are the most significantly altered. H2A.Zac transiently elevates at the nuclear periphery of hESCs just prior to loss of pluripotency, but is then lost; whereas from day 2 of differentiation, H3K9me2 becomes peripherally elevated instead. We have shown that ongoing HDAC activity is responsible for removing H2A.Zac from the nuclear periphery at the onset of differentiation, and that HDAC activity is essential for differentiation to proceed.

From an analysis of the transcriptional activation and repression of the androgen receptor system (Ito et al., 2018; Valdés-Mora et al., 2017), Giaimo et al. (2019) have proposed that H2A.Z, and especially ubiquitylated H2A.Z, can be repressive, but H2A.Z acetylation leads to its deubiquitylation and consequent activation of genes. Our finding that the nuclear periphery is specifically and transiently enriched for H2A.Z acetylation in the early stages of pluripotency loss of hESCs suggests that, upon differentiation, many genes normally found at the periphery, a generally repressive compartment, may rapidly transit to an active state through the action of H2A.Z-specific acetyltransferases. While the current study

Journal of Cell Science (2020) 133, jcs245282. doi:10.1242/jcs.245282

does not identify the genes that may be so regulated, it predicts that many genes whose activation is regulated by H2A.Z acetylation during TBL differentiation are likely to be found in hESC lamin-associated domain (LAD) compartments.

Other studies have assayed the subnuclear distribution of histone modification marks, including H3K4me2 and me3, H3K9me1, me2 and me3, H3K9ac, H3K27me2 and me3 and H3K79me1, in pluripotent and differentiated hESCs induced to differentiate by non-directed means. These studies reported that the only histone modifications that exhibited changes in radial distribution were H3K9me3, H3K9ac and H3K79me1, which were described as being reduced at the nuclear periphery (Bártová et al., 2008). However, our results showed that H3K9ac and H3K9me3 showed no significant location differences as hESCs lose pluripotency. These discrepancies could arise from differences in differentiation protocols and fate (our TBL protocol versus non-directed differentiation) as well as the image analysis methods used to calculate peripheral enrichment. In our method, we define the periphery of the nucleus based on thresholded DAPI staining, using the same criteria for all nuclei in the study, and then assign shells by distance working inwards, as compared to the method employed by Bártová et al. (2008), wherein radial shells were established working outwards from the nucleus center. It is likely, however, that the particular histone marks enriched in the periphery vary, as commitment to different lineages involves different signals and transcriptional programs.

Treating primed hESC with the HDAC inhibitor TSA caused persistent and increased intensity of H2A.Zac throughout the nucleoplasm and at the nuclear periphery. This suggests that there is constant, active de- and re-acetylation in pluripotent ESCs. Taken together with a previous observation that very little redistribution of lamina-associated chromatin occurs within a single interphase (Kind et al., 2013), we think it likely that increase of peripheral H2A.Z acetylation is in large part controlled locally through modification of periphery-associated chromatin. However, rescrambling of peripheral associations in telophase (also shown in Kind et al., 2013) would tend to homogenize any persistent histone modifications, and this process likely contributes passively to removal of peripheral enrichment of H2A.Zac. Another factor that may influence the degree of observed signal increase or decrease is the density of DNA at the periphery. However, changes of DNA density at the periphery cannot be the sole cause of the enrichment we see, since some mechanism must act to control the timing of the two complementary modifications. In addition to persistent H2A.Zac at the periphery, the appearance of H3K9me2 at the periphery was correspondingly delayed in TSA-treated cells, suggesting that the two histone modifications are regulated by linked mechanisms that are triggered upon pluripotency loss. A limitation of our observations is that we cannot directly attribute delayed differentiation, nor delayed H3K9me2 enrichment, to the acetylation state of H2A.Z, since TSA is a broad-spectrum HDAC inhibitor with many potential targets.

In conclusion, we have shown evidence that the redistribution of two chromatin modifications (H2A.Zac and H3K9me2) at the nuclear periphery is a hallmark of pluripotency loss during differentiation toward a trophoblast state. We have shown that lamin A is not necessary for the successive enrichment of H2A.Zac and H3K9me2 at the periphery during TBL differentiation. We have also shown, through cytological analysis, that H2A.Zac negatively correlates with H3K9me2. As a contextual overview, we suggest that, in the naïve hESC, H3K9me2 exists at the periphery to reinforce the peripheral location of silenced genes. However, when the hESC enters a primed state, Tip60 (or another H2A.Z acetylase) activity is higher at the periphery, enabling H2A.Z to be rapidly acetylated at the periphery following HDAC reduction upon pluripotency loss. This could also prevent premature accumulation of H3K9me2 at the nuclear periphery, ensuring the proper restructuring of chromatin upon lineage commitment and the refinement of key regulating elements such as LADs. Future work using single-cell ChIP-Seq analysis of histone marks over time could determine the identity of the genes regulated by the peripheral changes we observe and give important clues into compartment-specific gene regulation during differentiation.

MATERIALS AND METHODS

Cell culture

Primary mouse embryonic fibroblast (MEF) cells (kindly provided by Norio Nakatsuji, iCeMS, Kyoto University, Japan) were grown under standard conditions (5% CO_2 humidified environment at 37°C) in DMEM supplemented with 10% fetal bovine serum. Human ESCs (H1 line, kindly provided by N. Nakatsuji) were maintained in ReproCell Primate medium supplemented with FGF2 StemBeads (8 µl/ml, Stem Cultures) on mitomycin-C inactivated MEFs, and mechanically passaged every 5–7 days. Following methods described in Gafni et al. (2013), hESCs were induced to a naïve state by growing cells in 'naïve human stem cell medium' (NHSM), which was ReproCell Primate medium containing LIF (20 ng/ml), TGFβ (1 ng/ml), FGF2 (8 ng/ml), PD0325901 (1 µM), CHIR99021 (3 µM), SP600125 (10 µM) and SB203580 (10 µM) (Gafni et al., 2013). NHSM was added to hESCs 3 days post passage, and cells were allowed to grow for 2 days before a subsequent passage. Cells were then grown for a further 5 days in NHSM and used as 'naïve' hESCs after the next passage. To differentiate hESCs into TBL cells, hESCs were passaged onto MEF-free surfaces coated with ESgrade Matrigel (Thermo Fisher Scientific, Cat# 354277) and grown in ReproCell FF2 medium and supplemented with FGF2 StemBeads. TBL differentiation was induced by removing hESC medium and growing cells with recombinant BMP4 (10 ng/ml), SB431542 (20 µM) and SU5402 (20 µM). For TSA treatments, TSA was added to the medium to a final concentration of 12.5 nM at 12 h after the start of differentiation induction. Cardiomyocyte differentiation of WT and *Lmna*$^{-/-}$ hESCs was performed using the inducing agent KY02111 following protocols in Minami et al. (2012). The hESC lines were used in accordance with the Guidelines for the Derivation and Utilization of Human Embryonic Stem Cells developed by the Ministry of Education, Culture, Sports, Science and Technology (MEXT), Japan. HeLa cells were cultured at 37°C in DMEM and checked routinely for contamination.

Immunofluorescence

For experiments, cells were seeded onto glass coverslips or 35 mm glass bottom dishes (Matsunami#1S) coated with ESgrade Matrigel (Thermo Fisher Scientific, Cat# 354277) and fixed by incubation with 4% paraformaldehyde (PFA) for 10 min at 4°C. Samples were washed with PBST (PBS with 0.1% Tween-20) and permeabilized with 0.5% Triton X-100 in PBS for 5 min at room temperature. Samples were washed again and incubated in blocking solution (2% BSA in PBST), then incubated with primary antibodies (Table S1) diluted in block solution in a humidified chamber overnight at 4°C. Samples were washed before incubation with secondary antibodies (Table S1) for 1 h at room temperature, washed again and counterstained with DAPI for 5 min before being mounted onto microscope slides with 1% *n*-propyl gallate in glycerol. Samples were stored at −20°C prior to imaging.

Peptide competition immunofluorescence assay

Synthesized modified peptides (Chinapeptide) were diluted in blocking solution at 10 µg/ml final concentration; the corresponding primary antibodies (H2A.Zac or H3K9me2) were added to this solution for primary incubation. Cells were incubated with the solution overnight at 4°C, after which the standard immunofluorescence procedure was continued. Peptide sequences of blocking peptides used were (from N to C terminus): H2A.Zac, AGGK(Ac)AGK(Ac)DSGK(Ac)AKAKAV; H3K9me2, ARTKQTARK-(me2)STGGKAPRK (Ac, acetylation; me2, dimethylation).

Journal of Cell Science (2020) 133, jcs245282. doi:10.1242/jcs.245282

RNA FISH

Cells were grown on glass coverslips and fixed as per the immunofluorescence procedure described above. FISH probes (Stellaris) directed against human *NANOG* and *CDX2* (see Table S2) were reconstituted in nuclease-free TE buffer to a concentration of 25 µM and stored at −20°C prior to use. Cells were permeabilized with cold 70% ethanol for 1 h before hybridization, washed in wash buffer [10% formamide in 2× saline-sodium citrate (SSC)] before hybridization was performed using probes diluted to 250 nM in hybridization buffer (10 mg/ml dextran sulfate and 10% formamide in 2× SSC) for 4 h at 37°C. Cells were then washed again, and nuclei were counterstained with DAPI in 2× SSC for 5 min before being mounted onto microscope slides with 1% *n*-propyl gallate in glycerol. Samples were stored at −20°C prior to imaging.

Fluorescence microscopy

Cells were imaged on a conventional wide-field DeltaVision personalDV deconvolution system (Applied Precision/GE Healthcare) using a 100×1.4NA oil objective and immersion liquid of refractive index 1.513 (Cargille). Images were corrected for bleaching and lamp flicker, and processed with constrained iterative deconvolution (Chen et al., 1995), using the softWoRx suite (Applied Precision/GE Healthcare). Deconvolution was performed with a measured point spread function obtained from 100 nm green fluorescent latex beads taken at a *Z*-step size of 0.2 µm, to remove out-of-focus light (Hiraoka et al., 1990). Axial chromatic aberration of different wavelengths was corrected through sub-pixel shifting in the *Z* direction based on peak axial positions of multicolor beads. Inspection and quantitative analysis of images was performed with the Fiji/ImageJ suite (Schindelin et al., 2012) and GNU Octave (Eaton et al., 2020), and archived for figure creation with the Open Microscopy Environment (Allan et al., 2012; Blackburn et al., 2016).

Western immunoblotting

Whole-cell lysate was extracted by lysis of cells with RIPA buffer (150 mM NaCl, 1.0% NP-40, 0.5% sodium deoxycholate, 0.1% SDS, and 50 mM Tris-HCl pH 8.0) including a protease inhibitor cocktail (Nacalai, Cat#03969) supplemented with 10 mM NaF, 1 mM PMSF and 1 mM Na_3VO_4 at 4°C. Next, 10 µg of proteins were subjected to SDS-PAGE using premade gels (Bio-Rad, Cat#4561086), and transferred onto PVDF membranes. For loading controls performed on different gels, equal volumes of the same lysate were loaded to equivalent lanes, and gels were blotted under identical conditions. Membranes were blocked with 5% milk in TBST for 1 h at room temperature and incubated with primary antibodies (Table S1) diluted in block solution at 4°C overnight. Membranes were washed with TBST before incubation with HRP-labeled secondary antibodies (dilution 1:10,000) for 1 h, and washed again. Protein signals were detected with LAS4000 using an ECL reaction (Nacalai, Cat#02230-30 and #11644-40). Primary antibody dilutions used were: Oct3/4, 1:2000; G9a, 1:2000; HDAC2, 1:2000; GAPDH (Wako#010-25521), 1:5000.

Knockout of the *LMNA* gene

hESCs (H1) were thawed at P29 and transfected with 3.3 µM of hCas9D10A (Addgene #74495), and a gRNA/donor plasmid (pUC_lmnA_Neo_exn1_donor_fixed containing gRNA sequence GCAGGAGCTCAATGA-TCGCTTGG; whole plasmid sequence available upon request) using Lipofectamine 2000, as per instructions. Cells were rescued and grown in the presence of ROCK inhibitor overnight, then placed in normal hESC medium on Matrigel for 4 days. Subsequently, G418 was added at 200 µg/ml to select for Neo^+ cells. After 2–3 days, cells were passaged to plates containing inactivated feeder MEF cells. After four days of colony growth, individual colonies were picked and grown in 24-well plates. Colonies were then sampled and screened by PCR for deletion. To check for off-target edits, after establishment of the $LMNA^{-/-}$ cell line, PCR and sequencing was carried out on a selection of sites in coding regions containing the nearest homology to the gRNA sequence, and no changes were found (data not shown). Primers used to screen for deletion/insertion were lmnA_nested_fwd (5′-GGGACTGAAGGGGGAAGG-3′) and lmnA_out_rev (5′-CACTCTGCGTGTCTGGG-3′), which were expected to give a 2 kb band in WT cells but a 3.2 kb band in deletion cells.

Periphery distance analysis

For each nucleus, an absolute nuclear periphery was automatically determined based on a Gaussian-smoothed and thresholded (Otsu method) DAPI image. Calculating the Euclidean distance map inward from the threshold boundary and binning by 100 nm (1.56 pixel increments) generation of peripheral ‘shells’ of 100 nm each. Nuclei and their shells were manually inspected in automatically generated preview images, and rejected from analysis if the shells surrounded less or more than one single nucleus; no nuclei were rejected on any other basis. For each nucleus, we selected a subset of 20 shells beginning ∼500 nm outside the true periphery and covering a total of 2 µm (see Fig. 3A). The average fluorescence intensity of lamin A compares well with the peripheral distribution profile of DAPI staining, serving as an internal control for the shell analysis (Fig. S3). Code (GNU Octave and Perl) for automatic segmentation, display, and calculation of shell analysis is provided at a public repository (github.com/pmcarlton/shellanalysis).

Statistical analysis

All statistical analysis was performed using R version 3.4.4 (R Core Team, 2018) or GraphPad Prism version 6.0 h for Macintosh (GraphPad Software, La Jolla, California, USA). No statistical method was used to predetermine sample size. All experiments were performed on at least three independent samples (biological replicates) unless otherwise specified.

Acknowledgements

We thank H. Kimura for kindly providing monoclonal antibodies, N. Nakatsuji for guidance and resources in maintaining human ES cells, I. Minami for assistance with cardiomyocyte differentiation, and A. Sato for critical reading and helpful discussions. G.R.K. was supported by the JSPS Foreign Postdoctoral Scholar program, Grant-in-Aid 24-02079. The Institute for Integrated Cell-Material Sciences (WPI-iCeMS) was supported during this research by the World Premier International Research Center Initiative (WPI), MEXT, Japan.

Competing interests

The authors declare no competing or financial interests.

Author contributions

Conceptualization: G.R.K., P.M.C.; Methodology: G.R.K., K.H., P.M.C.; Software: P.M.C.; Validation: Y.T.; Investigation: G.R.K., Y.T., R.R.-B., E.S.; Resources: K.H.; Data curation: G.R.K., Y.T., R.R.-B., P.M.C.; Writing - original draft: G.R.K., P.M.C.; Writing - review & editing: G.R.K., Y.T., P.M.C.; Visualization: P.M.C.; Supervision: K.H., P.M.C.; Project administration: G.R.K., P.M.C.; Funding acquisition: P.M.C.

Funding

This project was carried out in part through funds provided by the Inamori foundation and the Sumitomo foundation.

Supplementary information

Supplementary information available online at
https://jcs.biologists.org/lookup/doi/10.1242/jcs.245282.supplemental

Peer review history

The peer review history is available online at
https://jcs.biologists.org/lookup/doi/10.1242/jcs.245282.reviewer-comments.pdf

References

Akhtar, A. and Gasser, S. M. (2007). The nuclear envelope and transcriptional control. *Nat. Rev. Genet.* **8**, 507-517. doi:10.1038/nrg2122

Allan, C., Burel, J.-M., Moore, J., Blackburn, C., Linkert, M., Loynton, S., Macdonald, D., Moore, W. J., Neves, C., Patterson, A. et al. (2012). OMERO: flexible, model-driven data management for experimental biology. *Nat. Methods* **9**, 245-253. doi:10.1038/nmeth.1896

Amita, M., Adachi, K., Alexenko, A. P., Sinha, S., Schust, D. J., Schulz, L. C., Roberts, R. M. and Ezashi, T. (2013). Complete and unidirectional conversion of human embryonic stem cells to trophoblast by BMP4. *Proc. Natl. Acad. Sci. USA* **110**, E1212-E1221. doi:10.1073/pnas.1303094110

Auger, A., Galarneau, L., Altaf, M., Nourani, A., Doyon, Y., Utley, R. T., Cronier, D., Allard, S. and Côté, J. (2008). Eaf1 is the platform for NuA4 molecular assembly that evolutionarily links chromatin acetylation to ATP-dependent exchange of histone H2A variants. *Mol. Cell. Biol.* **28**, 2257-2270. doi:10.1128/MCB.01755-07

Bártová, E., Galiová, G., Krejcí, J., Harničarová, A., Strašák, L. and Kozubek, S. (2008). Epigenome and chromatin structure in human embryonic stem cells undergoing differentiation. *Dev. Dyn.* **237**, 3690-3702. doi:10.1002/dvdy.21773

Journal of Cell Science (2020) 133, jcs245282. doi:10.1242/jcs.245282

Blackburn, C., Allan, C., Besson, S., Burel, J.-M., Carroll, M., Ferguson, R. K., Flynn, H., Gault, D., Gillen, K., Leigh, R. et al. (2016). The Open Microscopy Environment: open image informatics for the biological sciences. p. 991324. International Society for Optics and Photonics. doi:10.1117/12.2232291

Bruce, K., Myers, F. A., Mantouvalou, E., Lefevre, P., Greaves, I., Bonifer, C., Tremethick, D. J., Thorne, A. W. and Crane-Robinson, C. (2005). The replacement histone H2A.Z in a hyperacetylated form is a feature of active genes in the chicken. *Nucleic Acids Res.* **33**, 5633-5639. doi:10.1093/nar/gki874

Chawengsaksophak, K., de Graaff, W., Rossant, J., Deschamps, J. and Beck, F. (2004). Cdx2 is essential for axial elongation in mouse development. *Proc. Natl. Acad. Sci. USA* **101**, 7641-7645. doi:10.1073/pnas.0401654101

Chen, H., Swedlow, J. R., Grote, M., Sedat, J. W. and Agard, D. A. (1995). The collection, processing, and display of digital three-dimensional images of biological specimens. In *Handbook of Biological Confocal Microscopy* (ed. J. B. Pawley), pp. 197-210. Boston, MA: Springer US.

Chen, X., Skutt-Kakaria, K., Davison, J., Ou, Y.-L., Choi, E., Malik, P., Loeb, K., Wood, B., Georges, G., Torok-Storb, B. et al. (2012). G9a/GLP-dependent histone H3K9me2 patterning during human hematopoietic stem cell lineage commitment. *Genes Dev.* **26**, 2499-2511. doi:10.1101/gad.200329.112

Constantinescu, D., Gray, H. L., Sammak, P. J., Schatten, G. P. and Csoka, A. B. (2006). Lamin A/C expression is a marker of mouse and human embryonic stem cell differentiation. *Stem Cells* **24**, 177-185. doi:10.1634/stemcells.2004-0159

Delcuve, G. P., Khan, D. H. and Davie, J. R. (2012). Roles of histone deacetylases in epigenetic regulation: emerging paradigms from studies with inhibitors. *Clin. Epigenetics* **4**, 5. doi:10.1186/1868-7083-4-5

Dovey, O. M., Foster, C. T. and Cowley, S. M. (2010). Histone deacetylase 1 (HDAC1), but not HDAC2, controls embryonic stem cell differentiation. *Proc. Natl. Acad. Sci. USA* **107**, 8242-8247. doi:10.1073/pnas.1000478107

Eaton, J. W., Bateman, D., Hauberg, S. and Wehbring, R. (2020). GNU Octave version 5.2.0 manual: a high-level interactive language for numerical computations. https://www.gnu.org/software/octave/doc/v6.1.0

Gafni, O., Weinberger, L., Mansour, A. A., Manor, Y. S., Chomsky, E., Ben-Yosef, D., Kalma, Y., Viukov, S., Maza, I., Zviran, A. et al. (2013). Derivation of novel human ground state naive pluripotent stem cells. *Nature* **504**, 282-286. doi:10.1038/nature12745

Giaimo, B. D., Ferrante, F., Herchenröther, A., Hake, S. B. and Borggrefe, T. (2019). The histone variant H2A.Z in gene regulation. *Epigenetics Chromatin* **12**, 37. doi:10.1186/s13072-019-0274-9

Harr, J. C., Luperchio, T. R., Wong, X., Cohen, E., Wheelan, S. J. and Reddy, K. L. (2015). Directed targeting of chromatin to the nuclear lamina is mediated by chromatin state and A-type lamins. *J. Cell Biol.* **208**, 33-52. doi:10.1083/jcb.201405110

Hiraoka, Y., Sedat, J. W. and Agard, D. A. (1990). Determination of three-dimensional imaging properties of a light microscope system. Partial confocal behavior in epifluorescence microscopy. *Biophys. J.* **57**, 325-333. doi:10.1016/S0006-3495(90)82534-0

Hiratani, I., Ryba, T., Itoh, M., Yokochi, T., Schwaiger, M., Chang, C.-W., Lyou, Y., Townes, T. M., Schübeler, D. and Gilbert, D. M. (2008). Global reorganization of replication domains during embryonic stem cell differentiation. *PLoS Biol.* **6**, e245. doi:10.1371/journal.pbio.0060245

Ito, S., Kayukawa, N., Ueda, T., Taniguchi, H., Morioka, Y., Hongo, F. and Ukimura, O. (2018). MRGBP promotes AR-mediated transactivation of KLK3 and TMPRSS2 via acetylation of histone H2A.Z in prostate cancer cells. *Biochim. Biophys. Acta Gene Regul. Mech.* **1861**, 794-802. doi:10.1016/j.bbagrm.2018.07.014

Jamaladdin, S., Kelly, R. D. W., O'Regan, L., Dovey, O. M., Hodson, G. E., Millard, C. J., Portolano, N., Fry, A. M., Schwabe, J. W. R. and Cowley, S. M. (2014). Histone deacetylase (HDAC) 1 and 2 are essential for accurate cell division and the pluripotency of embryonic stem cells. *Proc. Natl. Acad. Sci. USA* **111**, 9840-9845. doi:10.1073/pnas.1321330111

Kar, M., Ghosh, D. and Sengupta, J. (2007). Histochemical and morphological examination of proliferation and apoptosis in human first trimester villous trophoblast. *Hum. Reprod.* **22**, 2814-2823. doi:10.1093/humrep/dem284

Keogh, M.-C., Mennella, T. A., Sawa, C., Berthelet, S., Krogan, N. J., Wolek, A., Podolny, V., Carpenter, L. R., Greenblatt, J. F., Baetz, K. et al. (2006). The Saccharomyces cerevisiae histone H2A variant Htz1 is acetylated by NuA4. *Genes Dev.* **20**, 660-665. doi:10.1101/gad.1388106

Kidder, B. L. and Palmer, S. (2012). HDAC1 regulates pluripotency and lineage specific transcriptional networks in embryonic and trophoblast stem cells. *Nucleic Acids Res.* **40**, 2925-2939. doi:10.1093/nar/gkr1151

Kim, H., Jang, M.-J., Kang, M.-J. and Han, Y.-M. (2011). Epigenetic signatures and temporal expression of lineage-specific genes in hESCs during differentiation to hepatocytes in vitro. *Hum. Mol. Genet.* **20**, 401-412. doi:10.1093/hmg/ddq476

Kind, J., Pagie, L., Ortabozkoyun, H., Boyle, S., de Vries, S. S., Janssen, H., Amendola, M., Nolen, L. D., Bickmore, W. A. and van Steensel, B. (2013). Single-cell dynamics of genome-nuclear lamina interactions. *Cell* **153**, 178-192. doi:10.1016/j.cell.2013.02.028

Lienert, F., Mohn, F., Tiwari, V. K., Baubec, T., Roloff, T. C., Gaidatzis, D., Stadler, M. B. and Schübeler, D. (2011). Genomic prevalence of heterochromatic H3K9me2 and transcription do not discriminate pluripotent from terminally differentiated cells. *PLoS Genet.* **7**, e1002090. doi:10.1371/journal.pgen.1002090

Minami, I., Yamada, K., Otsuji, T. G., Yamamoto, T., Shen, Y., Otsuka, S., Kadota, S., Morone, N., Barve, M., Asai, Y. et al. (2012). A small molecule that promotes cardiac differentiation of human pluripotent stem cells under defined, cytokine- and xeno-free conditions. *Cell Rep.* **2**, 1448-1460. doi:10.1016/j.celrep.2012.09.015

Mori, M., Ishikawa, G., Luo, S.-S., Mishima, T., Goto, T., Robinson, J. M., Matsubara, S., Takeshita, T., Kataoka, H. and Takizawa, T. (2007). The cytotrophoblast layer of human chorionic villi becomes thinner but maintains its structural integrity during gestation. *Biol. Reprod.* **76**, 164-172. doi:10.1095/biolreprod.106.056127

Niwa, H. (2014). The pluripotency transcription factor network at work in reprogramming. *Curr. Opin. Genet. Dev.* **28**, 25-31. doi:10.1016/j.gde.2014.08.004

O'Keefe, R. T., Henderson, S. C. and Spector, D. L. (1992). Dynamic organization of DNA replication in mammalian cell nuclei: spatially and temporally defined replication of chromosome-specific alpha-satellite DNA sequences. *J. Cell Biol.* **116**, 1095-1110. doi:10.1083/jcb.116.5.1095

Padeken, J. and Heun, P. (2014). Nucleolus and nuclear periphery: velcro for heterochromatin. *Curr. Opin. Cell Biol.* **28**, 54-60. doi:10.1016/j.ceb.2014.03.001

Peric-Hupkes, D., Meuleman, W., Pagie, L., Bruggeman, S. W. M., Solovei, I., Brugman, W., Gräf, S., Flicek, P., Kerkhoven, R. M., van Lohuizen, M. et al. (2010). Molecular maps of the reorganization of genome-nuclear lamina interactions during differentiation. *Mol. Cell* **38**, 603-613. doi:10.1016/j.molcel.2010.03.016

Poleshko, A., Smith, C. L., Nguyen, S. C., Sivaramakrishnan, P., Wong, K. G., Murray, J. I., Lakadamyali, M., Joyce, E. F., Jain, R. and Epstein, J. A. (2019). H3K9me2 orchestrates inheritance of spatial positioning of peripheral heterochromatin through mitosis. *Elife* **8**, e49278. doi:10.7554/eLife.49278

Puckelwartz, M. J., Depreux, F. F. and McNally, E. M. (2011). Gene expression, chromosome position and lamin A/C mutations. *Nucleus* **2**, 162-167. doi:10.4161/nucl.2.3.16003

R Core Team (2018). R: A Language and Environment for Statistical Computing. https://www.R-project.org/

Sachs, M., Onodera, C., Blaschke, K., Ebata, K. T., Song, J. S. and Ramalho-Santos, M. (2013). Bivalent chromatin marks developmental regulatory genes in the mouse embryonic germline in vivo. *Cell Rep.* **3**, 1777-1784. doi:10.1016/j.celrep.2013.04.032

Schindelin, J., Arganda-Carreras, I., Frise, E., Kaynig, V., Longair, M., Pietzsch, T., Preibisch, S., Rueden, C., Saalfeld, S., Schmid, B. et al. (2012). Fiji: an open-source platform for biological-image analysis. *Nat. Methods* **9**, 676-682. doi:10.1038/nmeth.2019

Schroeder, D. I., Blair, J. D., Lott, P., Yu, H. O. K., Hong, D., Crary, F., Ashwood, P., Walker, C., Korf, I., Robinson, W. P. et al. (2013). The human placenta methylome. *Proc. Natl. Acad. Sci. USA* **110**, 6037-6042. doi:10.1073/pnas.1215145110

See, K., Lan, Y., Rhoades, J., Jain, R., Smith, C. L. and Epstein, J. A. (2019). Lineage-specific reorganization of nuclear peripheral heterochromatin and H3K9me2 domains. *Development* **146**, dev174078. doi:10.1242/dev.174078

Sekhavat, A., Sun, J.-M. and Davie, J. R. (2007). Competitive inhibition of histone deacetylase activity by trichostatin A and butyrate. *Biochem. Cell Biol.* **85**, 751-758. doi:10.1139/O07-145

Solovei, I., Wang, A. S., Thanisch, K., Schmidt, C. S., Krebs, S., Zwerger, M., Cohen, T. V., Devys, D., Foisner, R., Peichl, L. et al. (2013). LBR and lamin A/C sequentially tether peripheral heterochromatin and inversely regulate differentiation. *Cell* **152**, 584-598. doi:10.1016/j.cell.2013.01.009

Sudheer, S., Bhushan, R., Fauler, B., Lehrach, H. and Adjaye, J. (2012). FGF inhibition directs BMP4-mediated differentiation of human embryonic stem cells to syncytiotrophoblast. *Stem Cells Dev.* **21**, 2987-3000. doi:10.1089/scd.2012.0099

Tachibana, M., Sugimoto, K., Nozaki, M., Ueda, J., Ohta, T., Ohki, M., Fukuda, M., Takeda, N., Niida, H., Kato, H. et al. (2002). G9a histone methyltransferase plays a dominant role in euchromatic histone H3 lysine 9 methylation and is essential for early embryogenesis. *Genes Dev.* **16**, 1779-1791. doi:10.1101/gad.989402

Therizols, P., Illingworth, R. S., Courilleau, C., Boyle, S., Wood, A. J. and Bickmore, W. A. (2014). Chromatin decondensation is sufficient to alter nuclear organization in embryonic stem cells. *Science* **346**, 1238-1242. doi:10.1126/science.1259587

Towbin, B. D., González-Aguilera, C., Sack, R., Gaidatzis, D., Kalck, V., Meister, P., Askjaer, P. and Gasser, S. M. (2012). Step-wise methylation of histone H3K9 positions heterochromatin at the nuclear periphery. *Cell* **150**, 934-947. doi:10.1016/j.cell.2012.06.051

Valdés-Mora, F., Gould, C. M., Colino-Sanguino, Y., Qu, W., Song, J. Z., Taylor, K. M., Buske, F. A., Statham, A. L., Nair, S. S., Armstrong, N. J. et al. (2017). Acetylated histone variant H2A.Z is involved in the activation of neo-enhancers in prostate cancer. *Nat. Commun.* **8**, 1346. doi:10.1038/s41467-017-01393-8

Warrier, S., Van der Jeught, M., Duggal, G., Tilleman, L., Sutherland, E., Taelman, J., Popovic, M., Lierman, S., Chuva De Sousa Lopes, S., Van Soom, A., (2017). Direct comparison of distinct naive pluripotent states in human embryonic stem cells. *Nat. Commun.* **8**, 15055. doi:10.1038/ncomms15055

Yoshida, M., Kijima, M., Akita, M. and Beppu, T. (1990). Potent and specific inhibition of mammalian histone deacetylase both in vivo and in vitro by trichostatin A. *J. Biol. Chem.* **265**, 17174-17179.